Available online at www.sciencedirect.com
ScienceDirect
Journal of Catalysis 252 (2007) 77–87
JOURNAL OF CATALYSIS
www.elsevier.com/locate/jcat

Combined liquid-phase ATR-IR and XAS study of the Bi-promotion in the aerobic oxidation of benzyl alcohol over Pd/Al_2O_3

Cecilia Mondelli [a,b,1], Davide Ferri [a,*,2], Jan-Dierk Grunwaldt [a], Frank Krumeich [a], Stefan Mangold [c], Rinaldo Psaro [d], Alfons Baiker [a,*]

[a] *Department of Chemistry and Applied Biosciences, ETH Zurich, Hönggerberg, CH-8093 Zurich, Switzerland*
[b] *Dipartimento di Chimica Inorganica, Metallorganica e Analitica, Università degli Studi, via Venezian 21, I-20133 Milano, Italy*
[c] *Forschungszentrum Karlsruhe, Synchrotron Light Source ANKA, D-76021 Karlsruhe, Germany*
[d] *ISTM-CNR, via C. Golgi 19, I-20133 Milano, Italy*

Received 3 August 2007; revised 10 September 2007; accepted 11 September 2007

Abstract

A combination of *in situ* attenuated total reflection infrared (ATR-IR) spectroscopy and X-ray absorption spectroscopy (XAS) was applied to study the effect of Bi on the evolution of surface species and on the structure of a 0.75 wt% Bi–5 wt% Pd/Al_2O_3 catalyst during liquid-phase aerobic oxidation of benzyl alcohol. To correlate structure and catalytic performance, both spectroscopic techniques were coupled with online measurements of the catalytic activity using FTIR spectroscopy. Compared with 5 wt% Pd/Al_2O_3, hardly any adsorbed CO was found in the infrared spectra of the Bi-promoted catalyst recorded under dehydrogenation conditions. This indicates that the major effect of Bi on surface species is to block sites responsible for benzaldehyde decarbonylation. XAS showed that both Bi and Pd are in the reduced state under these conditions, as in the unpromoted catalyst. Under aerobic conditions, both ATR-IR and XAS indicated that Bi controls the supply of oxygen to the noble metal. As a consequence, the Bi-promoted Pd/Al_2O_3 catalyst was more resistant against overoxidation and thus was active for longer time on stream in the presence of an excess of oxygen. Pd remained in the metallic state over a wide range of experimental conditions. Reoxidation was found only after feeding an alcohol-free oxygen-saturated solution and was associated with lower catalytic activity when the alcohol was readmitted under aerobic conditions. Finally, the formation of carboxylates from benzaldehyde hydration/oxidation was largely hindered in the presence of Bi. This study demonstrates the potential of the combination of the two techniques, which allows drawing conclusions on both the particle structure/oxidation state (by XAS) and the surface species (by ATR-IR), and thus a correlation with catalytic performance.

Keywords: Promoter effect; Bismuth; Alcohol oxidation; Palladium; Liquid phase; ATR-IR; XAS; *Operando* spectroscopy

1. Introduction

Supported palladium nanoparticle catalysts applied in fine chemical synthesis are often combined with a second metal to improve catalytic activity and selectivity. An example of an important class of reactions is the selective oxidation of alcohols to carbonyls [1,2]. The use of molecular oxygen is an attractive "green" technology for the production of key intermediates in the fragrance and pharmaceutical industries. Typical bimetallic formulations include combinations with Bi or Pb [3,4] and, more recently, Au [5–9]. The promoter metal improves the performance and lifetime of the oxidation catalyst, prevents catalyst deactivation [10], and modifies the product distribution, thereby strongly influencing selectivity [11–13]. The nature of this effect remains under debate; one reason for this is that the origin of the promotion is complex and the result of numerous superimposed effects [1,2]. Feasible models for the role of the metal promoter include (a) formation of a complex among the noble metal, promoter, and reactant; (b) geometric blocking;

* Corresponding authors.
E-mail addresses: davide.ferri@empa.ch (D. Ferri), baiker@chem.ethz.ch (A. Baiker).
[1] On leave from the Università degli Studi, Milano, Italy.
[2] Present address: Laboratory for Solid State Chemistry and Catalysis, Empa, Ueberlandstrasse 129, CH-8600 Dübendorf, Switzerland.

0021-9517/$ – see front matter
doi:10.1016/j.jcat.2007.09.013

(c) bifunctional catalysis; (d) alloy formation; (e) co-catalysis in which the promoter protects the noble metal; and (f) homogeneous catalysis on promoter leaching.

A simple discrimination of the discrimination effect on Pd- and Pt-containing catalysts [14] is based on a comparison of the catalytic performance of promoted and unpromoted catalysts in the absence of molecular oxygen (under dehydrogenation conditions) assuming the validity of the dehydrogenation mechanism [1,2,15]. In this approach, besides the possible role in regulating the oxygen transfer to the active metal, the function of the metal promoter is to influence the rate of dehydrogenation and/or to substantially change the product distribution under inert conditions.

Because of the liquid-phase environment in which alcohol oxidation is typically performed, it is preferable to use suitable spectroscopic methods for investigating the catalyst immersed in the liquid phase in its working state. Spectroelectrochemical methods have contributed to the present understanding of these processes, but are somewhat limited by the use of electrolytic solutions, base additives, and model catalysts [16–20]. X-ray absorption spectroscopy has proven to be a powerful tool for following the state of the metal *during* reaction [21] and also has been applied to investigate the origin of promotion [22,23]. The major effect of Bi in the oxidation of 1-phenylethanol and cinnamyl alcohol on Pd/Al_2O_3 was to protect Pd from oxidation and to act as a geometric promoter on the Pd particles.

To the best of our knowledge, to date no experimental observation of the possible difference in the evolution of surface species on the promoted and unpromoted supported noble metal catalyst during reaction has been given. Knowledge of the distribution of species on the catalyst surface is crucial for understanding how the metal promoter affects the complex reaction mechanism involved in alcohol oxidation. This molecular level of understanding can be achieved using a vibrational spectroscopy allowing for *in situ* and *operando* studies. One such spectroscopy is infrared spectroscopy in the internal reflection geometry (ATR-IR) [24,25]. This short path length technique allows the enhancement of sensitivity toward the solid–liquid interface, in the specific case of heterogeneous catalysis at the catalyst–solution interface. ATR-IR spectroscopy already has been successfully used to study the reaction mechanism of alcohol oxidation in some detail [26,27]. Recently, it also proved powerful in uncovering possible active sites involved in dehydrogenation- and decarbonylation-type reactions [28]. Decomposition of benzaldehyde, the product of benzyl alcohol oxidation on Pd/Al_2O_3, occurs predominantly on large Pd domains [likely (111) crystal faces]. This study indicated two strategies to improve selectivity: blocking these sites and decreasing the particle size and/or loading, or increasing dispersion of Pd in the commonly used 5 wt% Pd/Al_2O_3. Metal promotion obviously belongs to the former strategy.

In the present study, we compared 5 wt% Pd/Al_2O_3 and 0.75 wt% Bi–5 wt% Pd/Al_2O_3 during benzyl alcohol oxidation in cyclohexane, with the aim of gaining insight into the possible role of the Bi-promoter on the evolution of the products and the stability of palladium against overoxidation. ATR-IR spectroscopy provides information on the surface processes at a molecular level, whereas XAS provides information on structural changes of the catalyst. Both techniques were coupled with online product monitoring using transmission FTIR spectroscopy to correlate the spectroscopic results directly with the catalytic performance.

2. Experimental

2.1. Materials

Benzyl alcohol (Aldrich, >99%), high-purity water (Merck) and cyclohexane solvent (Acros, >99%) were used as received. Synthetic air, hydrogen, CO, and Ar were of 99.999 vol% grade (PANGAS). Al_2O_3 (Fluka, for chromatography) was used as a reference material. The textural properties of the 5 wt% Pd/Al_2O_3 (Johnson Matthey 324) catalyst have been reported elsewhere [29]. The bimetallic 0.75 wt% Bi–5 wt% Pd/Al_2O_3 (herein $Pd–Bi/Al_2O_3$) catalyst was prepared as described elsewhere [23]. The effective loading of the Bi-promoter was estimated from the edge jump in the XANES spectra at the Bi L_3-edge [14].

2.2. Electron microscopy

For scanning transmission electron microscopy (STEM), the material was dispersed in ethanol and deposited onto a perforated carbon foil supported on a copper grid. The investigations were performed on a Tecnai F30 microscope [FEI (Eindhoven) with a field emission cathode, operated at 300 kV]. STEM images, obtained with a high-angle annular dark field (HAADF) detector, revealed the areas containing heavier elements (here Bi) with bright contrast (Z contrast). The focused electron beam was then set on selected spots to analyze the composition qualitatively by energy-dispersive X-ray spectroscopy [EDXS; detector (EDAX) attached to the Tecnai F30 microscope].

2.3. Attenuated total reflection infrared spectroscopy

A home-built stainless steel flow-through cell equipped with two independent flow channels was used throughout the experiments [30]. To prepare independent powder films, the trapezoidal ZnSe internal reflection element (IRE, bevel of 45°, $52 \times 20 \times 2$ mm, Crystran Ltd) was inserted into a mask. Aqueous slurries of the catalytic materials were pipetted into the channels of the mask on the large face of the IRE. After evaporation in air, the films homogeneously covered the geometric area of each channel (ca. 40×7 mm) with a thickness of about 10 μm, as determined from cross-sectional SEM images.

After mounting, the cell was fixed on the movable stage of a dedicated mirror unit (Optispec) within the sample compartment of the FTIR spectrometer (Equinox 55, Bruker Optics) equipped with an MCT detector. The computer-controlled stage (Fig. 1A) was moved alternatively up and down to align the corresponding channel with the focused infrared beam, thus completing a dual-channel experiment analogous to a single-beam single-reference (SBSR) experiment [31,32]. Thus, information was obtained from both channels nearly simultaneously

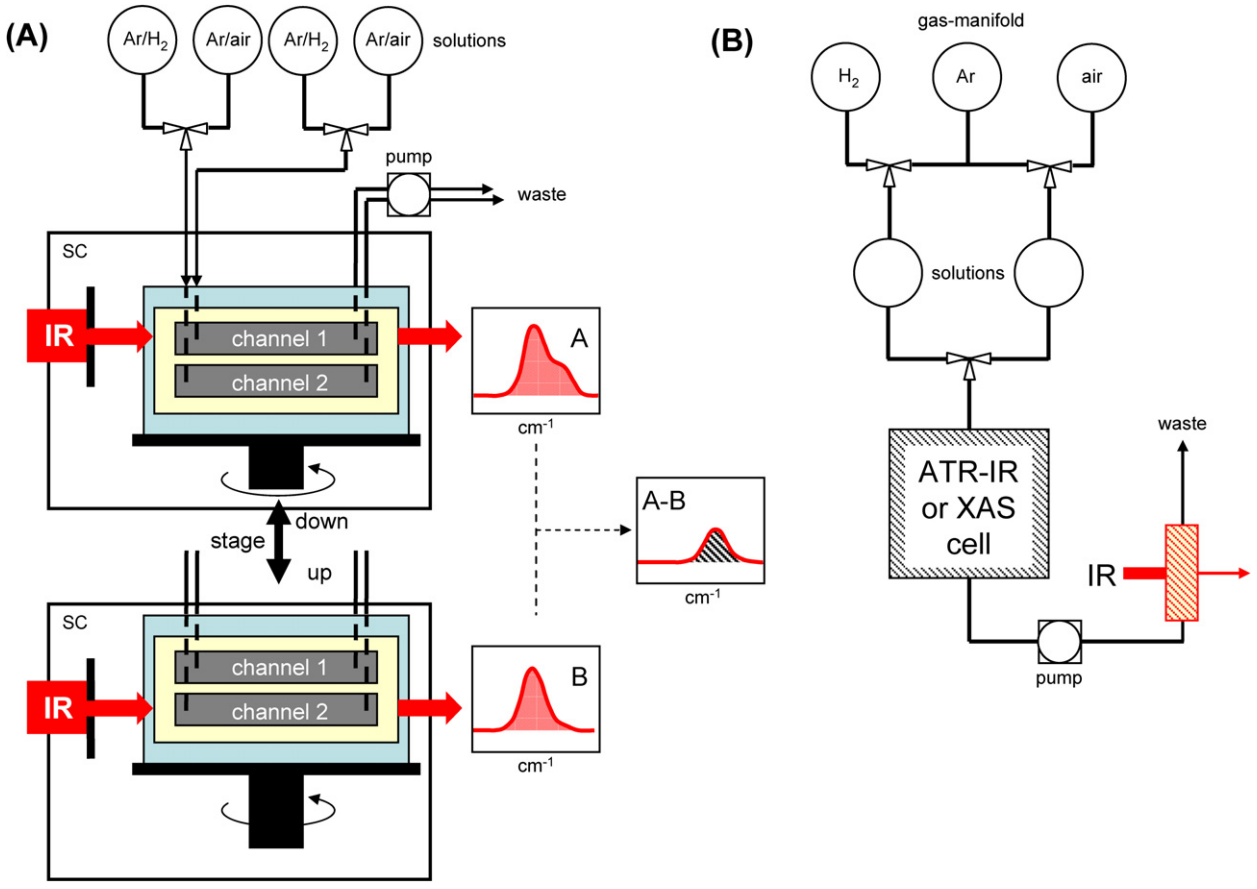

Fig. 1. (A) Experimental set-up for dual channel ATR-IR measurements. SC: sample compartment. (B) Experimental setup for both XAS and (single channel) ATR-IR measurements with integrated on-line FTIR monitoring of the effluent of the cell.

(ca. 40 s time lag). All ATR-IR spectra were recorded by averaging 200 scans at a 4-cm^{-1} resolution. The spectra are presented in absorbance units, where the last spectrum obtained during *in situ* reduction of the catalyst serves as the reference. Where required, spectra were corrected to compensate for the absorption of atmospheric water.

Cyclohexane solvent and alcohol solutions (20 mM) saturated with different gases were provided from two pairs of glass bubble reservoirs connected to the two independent inlets of the cell (Fig. 1A). Two reservoirs were used for Ar and hydrogen, and the two others contained a solution of the alcohol to be saturated by Ar and then air. Two pneumatically activated Teflon valves installed at the inlets of the cell were used to select the appropriate solution from a reservoir. The flows were regulated at a liquid flow rate of 0.65 ml/min using a peristaltic pump (Reglo 100, Ismatec) located after the cell. Stainless steel tubing was used throughout. All experiments were carried out at 50 °C.

The following protocol was used for both single-channel and dual-channel experiments. After Ar-saturated cyclohexane was admitted to the two flow channels for 60 min, Ar was replaced by hydrogen in the two reservoirs, and the catalysts were reduced *in situ* by flowing H_2-saturated cyclohexane for 30 min. Then the reaction was started by supplying solutions of benzyl alcohol saturated with Ar to the catalysts. After 30 min, Ar was replaced by air in the same reservoirs, and the air-saturated solution of the alcohol was contacted with the catalyst coating for ca. 60 min. The signal of the targeted product benzaldehyde at 1713 cm^{-1} [ν(C=O)] was integrated using the OPUS software package.

In the case of CO adsorption from the liquid phase, CO-saturated cyclohexane was fed to the cell after *in situ* reduction in a single-channel experiment.

2.4. Diffuse reflectance infrared spectroscopy

Diffuse reflectance measurements were performed with an Equinox 55 spectrometer (Bruker Optics) equipped with a HVC-DRP2 reaction chamber (Harrick) and an MCT detector. Samples were prepared by diluting the sample (10 mg) with KBr. CO adsorption was carried out at 50 °C by flowing 10 vol% CO/Ar at a flow rate of 10 ml/min after reduction at 300 °C in flowing hydrogen (10 vol% H_2/Ar) for 1 h. Spectra are reported in absorbance units without further correction.

2.5. X-ray absorption spectroscopy

The measurements were carried out at ANKA-XAS (2.5 GeV, injection current 140 mA) of the ANKA Synchrotron Laboratory (Forschungszentrum, Karlsruhe, Germany) in the transmission geometry using a Si(111) double crystal for monochromatization of the beam at the Bi L_3-edge. A continuous-

flow reactor cell (0.12 mL volume) moved into the X-ray beam using a x, z, θ stage and loaded with ca. 15 mg of catalyst was used [33]. The experimental setup (Fig. 1B) and protocol were analogous to those used for the ATR-IR measurements, except for the spectroscopic/reaction cell.

Three ionization chambers filled with an appropriate partial pressure of Ar (15% X-ray absorption in the first, 30% in the second and in the third ionization chamber) were used to record the intensity of the incident and the transmitted X-rays. The spectroscopic cell was located between the first and second chambers. The reference foil (Bi) for energy calibration was placed between the second and the third ionization chambers. Under stationary conditions, XANES spectra were taken around the Bi L_3-edge between 13.34 and 14.40 keV. Short EXAFS scans were recorded in the continuous scanning mode between 13.35 and 13.85 keV (Bi L_3-edge, typically ca. 2 min/scan). The raw data were energy-calibrated with the respective metal foil, background-corrected, normalized, and fitted using the WINXAS 3.1 software package [34].

Additional measurements were performed in the transmission geometry at HASYLAB, DESY (Hamburg, Germany) at beamline X1 to collect information around the Pd K-edge. XAS spectra were collected using a Si(311) double-crystal monochromator. The storage ring was operated at 4.45 GeV with injection currents of 150 mA. Higher harmonics were removed by detuning the crystals to 60% of the maximum intensity, and three ionization chambers (filled with Ar and Kr; see above) were used. The samples were located between the first and second ionization chambers; a reference sample (Pd-foil) was placed between the second and the third ionization chambers. EXAFS spectra of the as-prepared catalyst placed in the flow cell and also under stationary reaction conditions during the *in situ* experiments were obtained in the step-scanning mode around the Pd K-edge (24.35 keV) between 24.10 and 25.50 keV (typically 40 min/scan). During *in situ* studies under dynamic reaction conditions, faster scans between 24.32 and 24.5 keV were recorded in the step-scanning mode or by applying the continuous-scanning mode (typically 5 min/scan). The raw data were energy-calibrated (Pd-foil: 24.350 keV, first inflection point), background-corrected, and normalized. Fourier transformation for EXAFS data was applied to the k^3-weighted functions in the interval $k = 2$–12.8 Å^{-1}. Data fitting was performed in R-space using theoretical backscattering phases, and amplitudes were calculated with the ab initio multiple scattering code FEFF6.0 [35].

2.6. Online monitoring of products

The catalytic performance (rate, selectivity) in both the ATR-IR and XAS microreactor cells was monitored online using FTIR spectroscopy to avoid the need for repeated sampling for ex situ analysis (Fig. 1B). This allows performing a real *operando* experiment. In the case of ATR-IR measurements, auxiliary single-channel experiments to the dual-channel experiments were needed for this purpose.

The outlet of the *in situ* cell (ATR-IR, XAS) was connected to the inlet of the transmission infrared cell using 1/16 inch stainless steel tubing. Online measurements were triggered independently from the ATR-IR and XAS measurements. Typically, the online measurement was started at the end of the catalyst reduction. Transmission infrared spectra were collected in the 4000–1000 cm^{-1} spectral range every 30 s at 4 cm^{-1} resolution with a spectrometer equipped with a DTGS detector and a 1-mm flow-through liquid cell (CaF_2 windows). The spectrometer was either a facility provided by the ANKA Synchrotron Laboratory (Equinox 55, Bruker Optics) or a Tensor 27 (Bruker Optics) transferred to Hamburg in the case of the measurements at HASYLAB.

The amount of benzaldehyde product in the effluent of the *in situ* cell(s) was calibrated with solutions of known concentration applying the Lambert–Beer law. The same transmission infrared cell was used, which was kept closed to avoid any change in path length. GC analysis of the effluents of the ATR-IR cell during single-channel measurements also was carried out for comparison on a Thermo Quest Trace 2000 chromatograph, equipped with an HP-FFAP capillary column and a flame ionization detector (FID).

2.7. Batch reactor catalytic measurements

The catalytic performance was measured in a glass reactor as described elsewhere [36]. Briefly, catalytic tests were performed at 50 °C using ca. 55 mg of catalyst and 4.7 mmol benzyl alcohol in 10 mL of cyclohexane. The experiments were divided into a dehydrogenation phase (2 h) before admission of oxygen (50 mL/min) and an aerobic phase (4 h). Samples were obtained during and at the end of every experiment, filtered, and diluted with isopropanol for subsequent gas chromatography analysis (Thermo Quest Trace 2000 using a HP-FFAP capillary column and an FID). No other product than benzaldehyde was detected. Mesitylene (0.9 mmol) was added to the reaction mixture to serve as an internal standard for GC analysis.

3. Results

3.1. Characterization and catalytic behavior

The bimetallic catalysts were prepared by deposition of Bi on Pd/Al_2O_3, followed by mild liquid-phase reduction under inert atmosphere [23]. The promoter metal is typically deposited in the form of small particles and/or adatoms on the active noble metal, with a fraction covering the support as well [17,37]. The *in situ* liquid-phase reduction of the Bi salt during catalyst preparation [17] and the reduction before the catalytic tests are effective under mild conditions (50 °C) and prevent the material from further structural changes, such as alloying [38]. This procedure excludes any high-temperature reductive treatment (ca. 300 °C, H_2), in contrast to other procedures [39–42], and allows the preferential deposition of Bi on the noble metal.

XPS data indicate that Bi is in the reduced state and covers ca. 30% of Pd; however, about 27% of the Bi has a cationic character and likely is deposited as Bi_2O_3 on the alumina support [23]. The STEM image shown in Fig. 2 reveals that the

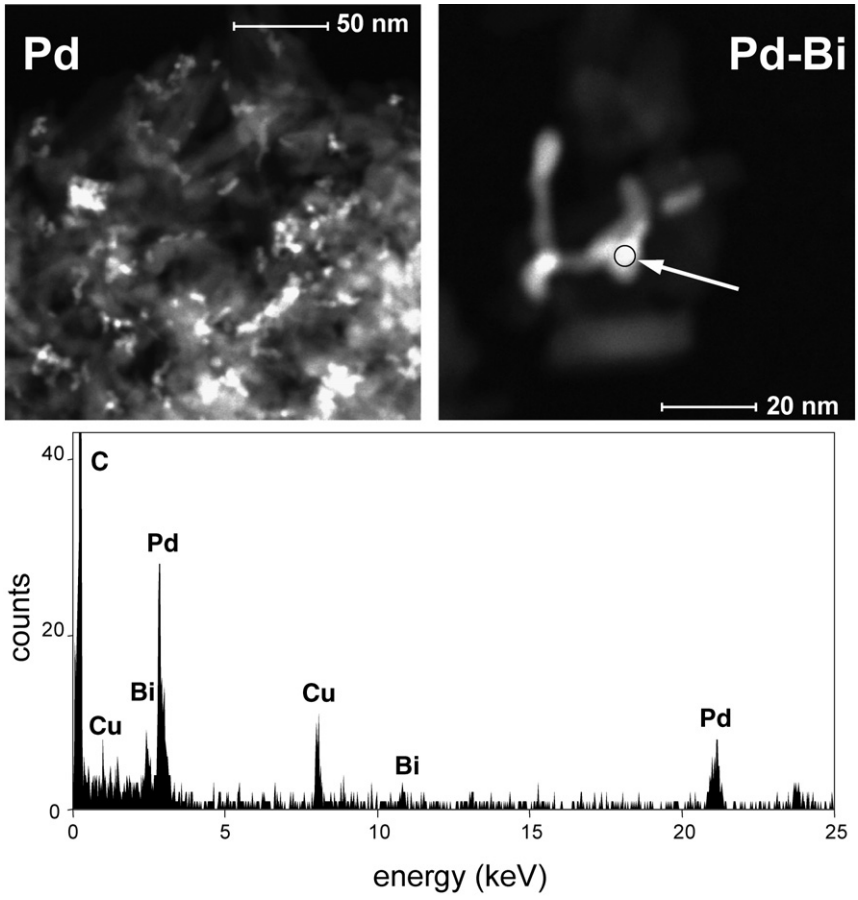

Fig. 2. HAADF-STEM images of Pd/Al_2O_3 and $Pd–Bi/Al_2O_3$ and EDX spectrum of a bimetallic aggregate. The EDX spectrum was recorded with the beam set on the spot indicated by the arrow in the corresponding STEM image.

metal particles in Pd/Al_2O_3 are arranged in aggregates over the support grains. This morphology and the particle size (average 3.4 nm) [27,29] were preserved after Bi addition. Importantly, EDX analysis pointed to the existence of both Pd and Bi at the same sampling point. Together with the likely absence of an alloy, this information indicates that Bi is deposited predominantly on Pd, thus confirming earlier XPS and EXAFS data [23].

CO adsorbed from the gas phase on Pd/Al_2O_3 reduced at 300 °C (Fig. 3) exhibits strong signals at 1982 and 1913 cm^{-1} and a weaker feature at 2083 cm^{-1}, which are associated with CO_{B2} [two-fold bridge CO on (100) faces and particle edges], CO_{B3} [three-fold CO on (111) faces], and CO_L (on top CO mainly on particle edges), respectively. The assignment is made according to the spectroscopic data available for supported Pd catalysts [43,44] and for well-defined Pd model catalysts [45] and assuming that the Pd particles are cubo-octahedra [28,43]. In contrast, the spectrum of $Pd–Bi/Al_2O_3$ reduced at 300 °C (Fig. 3) is dominated by the intense signal of CO_L (2085 cm^{-1}), with some contribution from bridged CO at 1967 and 1886 cm^{-1}. Although this sample has not been characterized further, the dramatic change in the distribution of adsorption sites on addition of Bi can be interpreted as resulting from the increase in surface defects induced by formation of a Pd–Bi alloy [39].

Adsorption of CO from the liquid phase after mild reduction at 50 °C displays significant differences with respect to adsorption from the gas phase [28]. Fig. 3 shows the ATR-IR spectra recorded after 1 h contact with CO. Two main signals are observed at 2078 and 1968 cm^{-1} on both catalysts, which are readily attributed to CO_L and CO_{B2}, respectively. The position of these signals is changed slightly compared with the gas-phase adsorption. Importantly, CO_{B3} species (shoulder at ca. 1870 cm^{-1}) are populated, but far less than on the sample reduced at 300 °C, likely because of the milder reduction conditions applied in the liquid phase. The weak signal at 2116 cm^{-1} indicates cationic $Pd^{\delta+}$ species [46]. Accordingly, EXAFS measurements showed that Pd hydride can be formed on Pd/Al_2O_3 under these conditions but is decomposed above 80–100 °C. Comparison of the ATR-IR spectra of CO adsorbed on Pd/Al_2O_3 [Fig. 3c] and $Pd–Bi/Al_2O_3$ [Fig. 3d] catalysts demonstrates that the signals are mostly unperturbed in terms of energy position; however, the CO_L/CO_{B2} ratio decreases from the monometallic sample to the Bi-containing sample. The generally lower signal intensity in $Pd–Bi/Al_2O_3$ suggests that the addition of Bi affects the availability of the metal surface for CO adsorption, which is in agreement with a fraction of Bi covering the metal particles and thus blocking adsorption sites. This behavior is also in agreement with the high reducibility of bismuth reported for these materials [23].

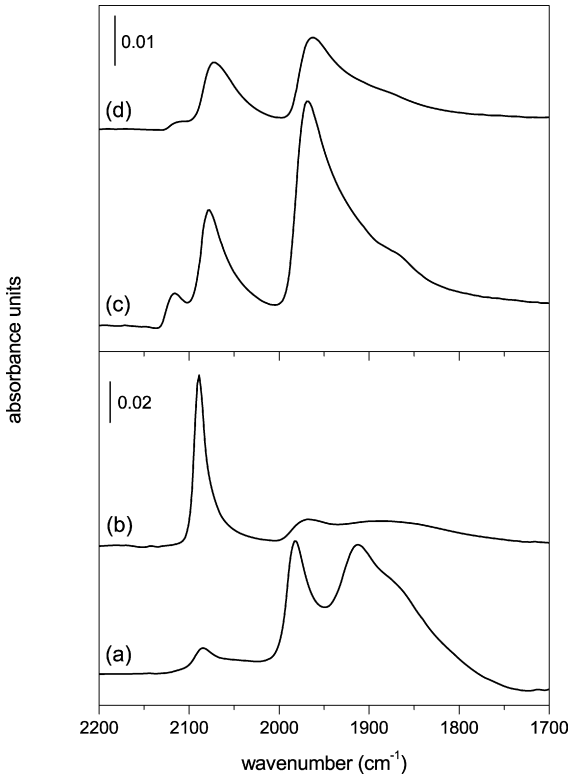

Fig. 3. DRIFT spectra of CO adsorption on (a) Pd/Al_2O_3 and (b) $Pd–Bi/Al_2O_3$ reduced at 300 °C in flowing hydrogen. Signals of gas-phase CO have been subtracted. Conditions: 50 °C, 10 mL/min flow rate, 1 h. ATR-IR spectra of CO adsorption over (c) Pd/Al_2O_3 and (d) $Pd–Bi/Al_2O_3$. Conditions: cyclohexane solvent, 50 °C, 1 h.

Table 1
Conversion (%) of benzyl alcohol for Pd/Al_2O_3 and $Pd–Bi/Al_2O_3$ after admittance of oxygen in the batch reactor. See Section 2.7 for reaction conditions. Benzaldehyde was found as the only product by GC analysis

Sample	Sampling time (h)			
	0[a]	0.5	2	4
5 wt% Pd/Al_2O_3	2	11	33	90
0.75 wt% Bi–5 wt% Pd/Al_2O_3	6	45	82	92

[a] Initial conversion value after 2 h reaction under dehydrogenation conditions prior to admittance of oxygen.

It is obvious from comparison of the gas-phase and liquid-phase CO adsorption that alloy formation does not occur in the as-prepared bimetallic catalysts owing to the mild liquid-phase reduction. After the addition of Bi, extended domains of Pd atoms remain exposed to the liquid phase and to the reactants.

Table 1 summarizes the catalytic behavior of Pd/Al_2O_3 and $Pd–Bi/Al_2O_3$ in the oxidation of benzyl alcohol under aerobic conditions. Before the admittance of oxygen, the catalysts were subjected to dehydrogenation conditions, under which a very low activity was found (time 0 h in Table 1). The catalytic data clearly indicate that $Pd–Bi/Al_2O_3$ was more efficient after the oxidant was admitted to the batch reactor. No other products were detected under aerobic conditions. Although the same level of conversion was attained after 4 h, $Pd–Bi/Al_2O_3$ exhibited a sudden increase in activity after admittance of oxygen, whereas Pd/Al_2O_3 reacted more slowly. This dramatic influence of Bi on the catalytic behavior of Pd under aerobic conditions has not been reported for other alcohols, but resembles that of Bi-promoted Pt/Al_2O_3 in the oxidation of cinnamyl alcohol [14].

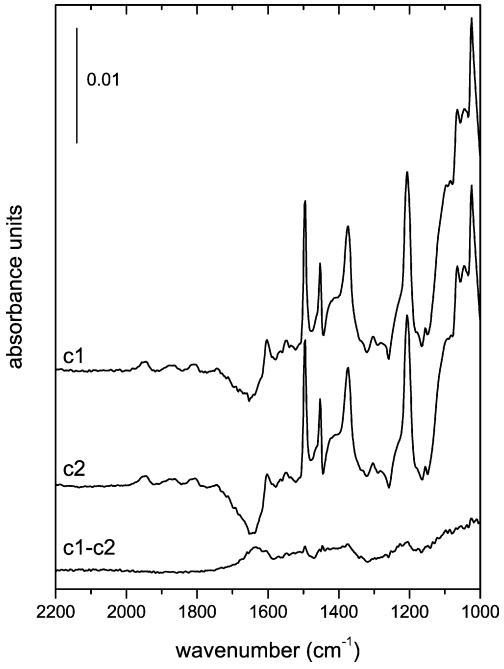

Fig. 4. ATR-IR spectra of a solution of benzyl alcohol on Al_2O_3 in the two channels of the cell (c1 and c2) and the corresponding difference spectrum (c1 − c2). Conditions: cyclohexane solvent, $C_{alcohol} = 0.02$ M, 50 °C, 1 h.

3.2. *In situ* ATR-IR and XAS study of benzyl alcohol oxidation

A substantial insight into the influence of Bi promotion on the evolution of species at the catalyst surface is obtained by monitoring the two catalysts at work. The dual-channel infrared experiments allow monitoring Pd/Al_2O_3 and $Pd–Bi/Al_2O_3$ nearly simultaneously under (close to) identical reaction conditions, both materials with identical histories. To validate the method, a series of ATR-IR spectra was measured in both channels of the cell on two identical particulate films of alumina during admission of benzyl alcohol in cyclohexane (Fig. 4). The SBSR spectrum obtained by subtracting the spectrum recorded in channel c2 from that recorded in channel c1 (c1 − c2, Fig. 4) displays only weak signals, which can be attributed simply to the time lag between the acquisition of the spectra in c1 and c2. This is best represented by the positive signal of adsorbed water (ca. 1630 cm^{-1}), which is slowly removed (negative signal in c1 and c2) on interaction of the alcohol with the alumina surface. Spectrum c1 exhibits a larger contribution from water, only because it was acquired before spectrum c2. Thus, it is reasonable to assume that the information is identical in the two channels and does not suffer from artifacts.

In situ ATR-IR spectroscopy and XAS on the $Pd–Bi/Al_2O_3$ catalyst combined with online catalytic data were applied to gain more insight into the origin of metal promotion from the viewpoint of the evolved surface species and the state of the metal components *during* the catalytic reaction. To the

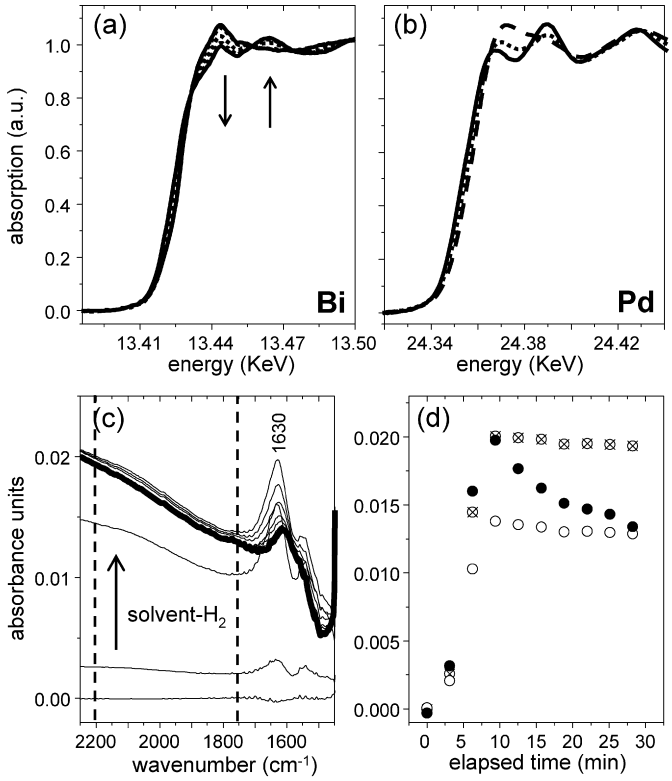

Fig. 5. XANES spectra at the Bi L_3-edge (a) and Pd K-edge (b) recorded during liquid-phase reduction of the Pd–Bi/Al_2O_3 catalyst in H_2-saturated solvent. The solid spectra at the Bi L_3-edge correspond to the beginning and the end of the reduction. The dotted and solid spectra at the Pd K-edge correspond to the beginning and the end of the reduction, respectively. The dashed line is the XANES spectrum of unreduced Pd/Al_2O_3. Conditions: cyclohexane solvent, 50 °C. (c) ATR-IR spectra recorded during *in situ* reduction of Pd–Bi/Al_2O_3 with H_2-saturated solvent. The arrow indicates the direction of the changes. Vertical dashed lines indicate two arbitrary points (2200 and 1750 cm^{-1}) belonging to the baseline. The last spectrum recorded during this treatment is bold. (d) Kinetics of the changes observed in (c) for the following frequencies: (⊗) 2200, (○) 1750 and (●) 1630 cm^{-1}. Conditions: cyclohexane solvent, 50 °C.

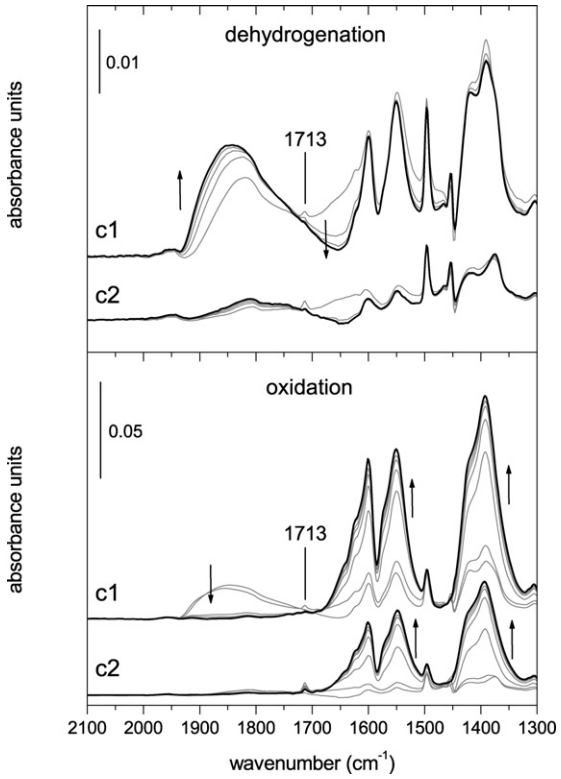

Fig. 6. ATR-IR spectra of a solution of benzyl alcohol in Ar- (top panel, 30 min) and air-saturated cyclohexane (bottom panel, 1 h) over Pd/Al_2O_3 (c1) and Pd–Bi/Al_2O_3 (c2). Bold spectra in c1 and c2 correspond to the last spectrum recorded before changing from Ar to air and from air to solvent flow. Time difference between displayed spectra in c1 and c2 is 5 min. The arrows indicate the (increasing-decreasing) trends of specific portions of the spectra. Conditions: cyclohexane solvent, $C_{alcohol} = 0.02$ M, 50 °C.

best of our knowledge, this combination and the combination with simultaneous catalytic activity measurements by FTIR has not been reported to date. Before admission of benzyl alcohol to the catalysts, the two materials were treated *in situ* with H_2-saturated solvent. This procedure affords reduced Pd (and Bi [23]) and is required for optimal catalytic performance, because oxidic palladium is less active [21]. Fig. 5 shows the changes observed by X-ray absorption and ATR-IR spectroscopy, indicating the reduction of the promoted noble metal particles in both cases. The change in the white line of the XANES spectra collected around the Bi L_3- and the Pd K-edges [Figs. 5a and 5b] shows that both metals are effectively reduced under these mild conditions. The spectra around the Bi L_3-edge were measured in the fast scan mode to preferentially follow the behavior of Bi. Identical results have been obtained with Pd/Al_2O_3 (not shown, cf. Ref. [21]). Fig. 5b shows that Pd is already more reduced in the fresh promoted catalyst than in Pd/Al_2O_3 and is further reduced in the presence of dissolved hydrogen. During treatment with H_2-saturated solvent, changes are observed in the ATR-IR spectra as well. Fig. 5c shows a general increase in the baseline (extending over the entire 4000–1000 cm^{-1} spectral region) of the spectra of Pd–Bi/Al_2O_3 (and Pd/Al_2O_3, not shown) which levels off after about 10 min. This change is attributed to a surface reduction process [30]. In addition, a signal of water evolves at ca. 1630 cm^{-1}, whose intensity passes through a maximum concomitant with the achievement of the saturation level in the offset of the baseline (Fig. 5d). The phenomena of water production and baseline offset are closely related and witness the reduction of Pd. After reduction of the surface oxide, water is formed more slowly or to a lesser extent and is preferentially desorbed from the catalyst.

Fig. 6 shows the typical ATR-IR spectra of benzyl alcohol on Pd/Al_2O_3 (c1) collected under dehydrogenation (Ar) and oxidative (air) conditions. Detailed assignment and discussion of the spectral features has been reported elsewhere [27,28]. Signals associated with dissolved benzaldehyde (1713 cm^{-1}), CO_{B3} (ca. 1843 cm^{-1}) and benzoate species (1600, 1575, 1548, 1497, 1422, and 1395 cm^{-1}) are detected during dehydrogenation. After admission of air, enhanced catalytic activity is observed from the increase in the intensity of the signal at 1713 cm^{-1} in both the ATR-IR and the online IR spectra. These effects are accompanied by the removal of adsorbed CO and additional accumulation of benzoate species.

The intensity and shape of the signal of CO_{B3} species is strikingly different from that observed during CO adsorption

from the liquid phase (Fig. 3). During CO adsorption, only a shoulder of the main CO_{B2} signal is observed, and the intensity of the CO_{B3} signal is much higher during reaction and is more comparable with the signal observed on a sample reduced at 300 °C before CO adsorption. A tentative interpretation of this fact, as demonstrated by the XAS measurements [23], is that the mild reduction at 50 °C in the liquid phase may afford Pd-hydride species. In the presence of benzyl alcohol, these hydrides are decomposed, and the properties of the metal surface are changed to such an extent so as to resemble that obtained after reduction at high temperature, at least from the standpoint of CO adsorption.

Surprisingly, the spectra recorded on Pd/Al_2O_3 and $Pd–Bi/Al_2O_3$ exhibit important differences over the entire spectral range reported in Fig. 6 under both dehydrogenation and oxidative conditions, indicating that Bi has a strong influence on the reaction network. The spectra in c2 ($Pd–Bi/Al_2O_3$) display a negligible amount of CO and less intense benzoate features in the absence of oxygen. Therefore, Bi inhibits decarbonylation of the product benzaldehyde and its further oxidation to benzoic acid, thus improving selectivity due to suppression of these two side reactions. The promoting effect is already manifest under dehydrogenation conditions. The lower extent of product oxidation on $Pd–Bi/Al_2O_3$ can be attributed either to an intrinsically poor hydrophilicity of the promoted system, due to Bi partially covering the Pd and Bi_2O_3 deposited on Al_2O_3, or simply to a diminished exposure of specific adsorption sites due to the presence of Bi (geometric effect) [22]. Careful inspection of the spectra also indicates that the intensity of the signal at 1713 cm^{-1} [ν(C=O)] is comparable on both materials under dehydrogenation conditions. This is best seen in Fig. 7, which reports the integrated area of this signal. The profiles match those obtained in independent single-channel experiments with online monitoring by FTIR (not shown). The maximum yield for the two catalysts is about 10%.

On replacement of Ar by air, the signals in the 1750–1300 cm^{-1} spectral region are enhanced [27]. The spectra acquired after 1 h reaction under oxidative conditions exhibit only differences related to the intensity of the signals of the benzoate species. This species is again formed more abundantly on Pd/Al_2O_3. Spectra in c1 (Fig. 6) show that CO is formed when air is admitted, but later it is completely displaced or oxidized. The intensity of the benzoate signals reaches saturation after about 1 h. Interestingly, the signal at 1713 cm^{-1} appears stronger on $Pd–Bi/Al_2O_3$ but reaches a maximum and then decreases in both materials. The saturation of the benzoate species, the disappearance of CO, and the attenuation of the signal of dissolved benzaldehyde with time clearly indicate that the liquid flow rate is high enough to allow excessive oxygen supply to the metal. Consequently, the rate of the reactions involved in the main catalytic cycle decreases over time, and high activity cannot be maintained over a long period (overoxidation) [47,48]. This again is best seen when comparing the behavior of the signal at 1713 cm^{-1} for both catalysts (Fig. 7). The profiles are clearly different in the oxidative phase (air) but similar under dehydrogenation conditions (Ar). In argon, benzaldehyde production passes through a maximum and then decreases as fast as the catalyst deactivates. The ATR-IR spectra indicate that CO is the main side product observed at this stage, but the metal surface is likely covered by hydrogen as well. A similar behavior with a maximum is observed under oxidative conditions (Fig. 7); however, in this case $Pd–Bi/Al_2O_3$ exhibits about threefold greater activity than the dehydrogenation phase and, importantly, a broader window of activity. The data shown in Fig. 7 reveal that Bi favors activity in the presence of oxygen (ca. 27% yield vs 17% of Pd/Al_2O_3), whereas the ATR-IR data in general strongly suggest that it favors selectivity (less adsorbed byproducts, i.e., CO and benzoates) and efficiency in both the absence and presence of oxygen.

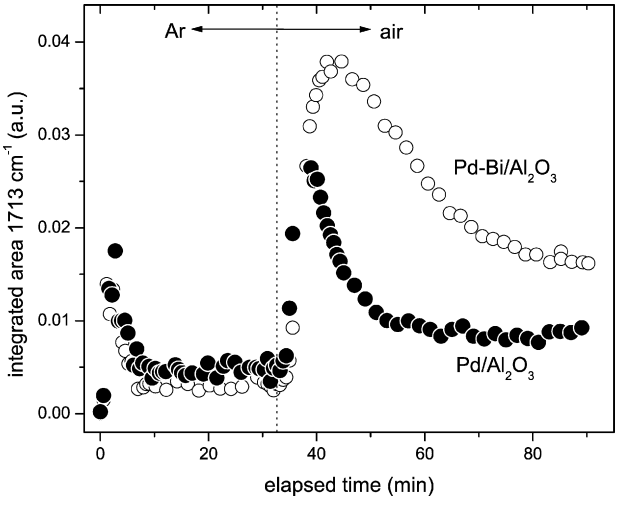

Fig. 7. Time-dependent profile of the integrated area of the signal at 1713 cm^{-1} (ν(C=O) of benzaldehyde) obtained from the dual channel ATR-IR experiment with Pd/Al_2O_3 and $Pd–Bi/Al_2O_3$ shown in Fig. 6.

In addition to the monitoring of the surface species evolving during reaction on the catalysts, the oxidation states of Bi and Pd were also followed during reaction using XANES by recording spectra in the fast mode (during changes of the reaction conditions) and EXAFS in the step-scanning mode (after steady-state conditions were reached). Because the Bi L_3-(13.42 keV) and Pd K-edge (24.35 keV) energies are rather far from one another, they do not interfere with the spectral region of the other component, thus allowing linear combination analysis to extract the oxidation state of the Bi species [23].

Fig. 8 depicts the changes in the activity observed during benzyl alcohol oxidation for $Pd–Bi/Al_2O_3$ as determined by online FTIR (intensity of the signal at 1713 cm^{-1}) and the corresponding change in the oxidation state of Bi. As mentioned above, Bi (and Pd; not shown) is readily reduced after H_2-saturated solvent is admitted into the XAS cell (Fig. 8, point 2). In agreement with the infrared data, low activity is detected under dehydrogenation conditions. As expected, the catalytic activity immediately increases when the reaction mixture is saturated with air (3) and O_2 (4), but the oxidation state of Bi (and Pd) is not perturbed.

In contrast to 1-phenylethanol, for which deactivation is observed with time on stream coincident with reoxidation of the Bi component [23], in the presence of benzyl alcohol, the catalytic activity was not significantly perturbed after the initial

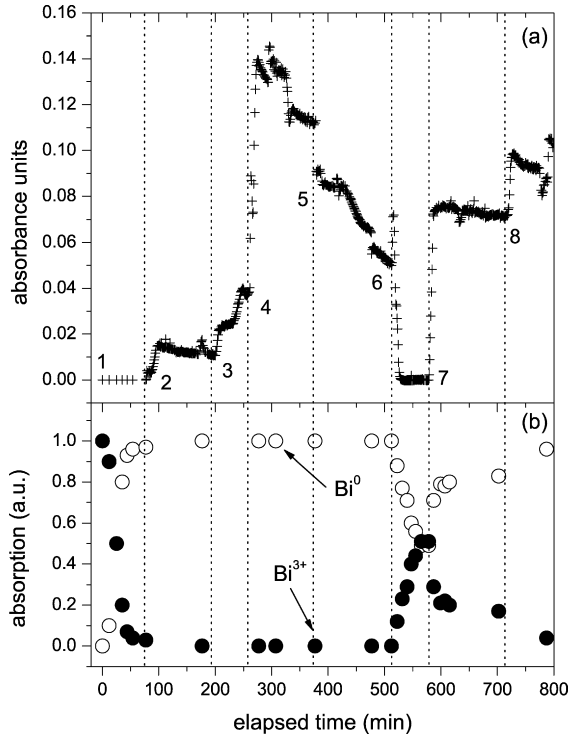

Fig. 8. Structure–performance relationships by combination of XANES and on-line FTIR for Pd–Bi/Al_2O_3. (a) Time-dependent profile of the intensity of the signal at 1713 cm^{-1} (benzaldehyde) and (b) change of the oxidation state of Bi determined from the linear combination of the XANES spectra recorded at the Bi L_3-edge. Conditions: cyclohexane solvent, $C_{alcohol} = 0.02$ M, 50 °C. Changes in experimental conditions are indicated in the top panel: (1) before H_2-saturated cyclohexane; (2) before benzyl alcohol in Ar-saturated cyclohexane; (3) before benzyl alcohol in air-saturated cyclohexane; (4) before benzyl alcohol in O_2-saturated cyclohexane; (5) temperature lowered to 30 °C; (6) before O_2-saturated cyclohexane; (7) before benzyl alcohol in O_2-saturated cyclohexane at 50 °C; (8) before increasing temperature to 60 °C.

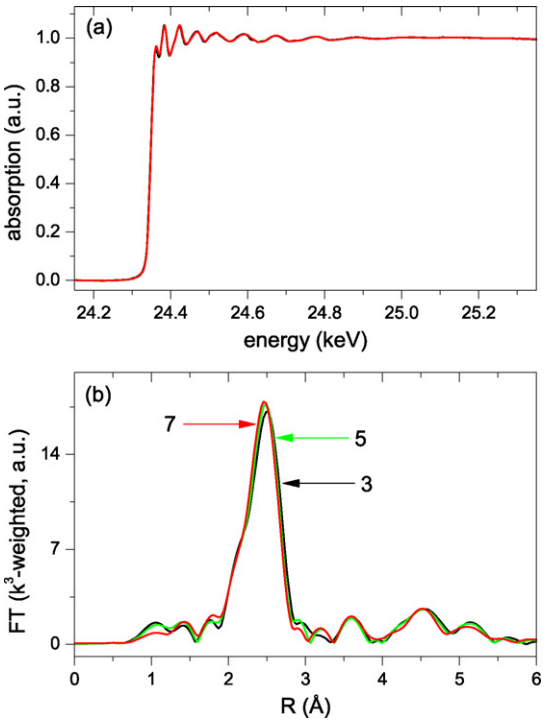

Fig. 9. Comparison of the (a) EXAFS spectra at the Pd K-edge and (b) the corresponding k^3-weighted Fourier transformed EXAFS spectra of Pd–Bi/Al_2O_3 at 50 °C. (3) With benzyl alcohol in Ar-saturated cyclohexane; (5) with benzyl alcohol in O_2-saturated cyclohexane at 30 °C, and (7) with O_2-saturated cyclohexane only.

increase. This can be traced to the more highly reducing character of benzyl alcohol. The spectra at the Pd K- and Bi L_3-edges show that both constituents are resistant to reoxidation, which for Bi is clear from the bottom panel of Fig. 8. The catalyst must be deactivated on purpose. Thus, first the temperature was lowered to 30 °C (5) in the presence of the alcohol [which, however, did not affect the oxidation state of Bi (and Pd)], and then the feed was replaced by O_2-saturated solvent (6). Obviously, the catalytic activity dropped to zero after exclusion of benzyl alcohol and about 50% of Bi was reoxidized. After partial reoxidation in O_2-saturated cyclohexane, significantly lower catalytic activity was observed when the alcohol was readmitted into the cell in the presence of oxygen (7) compared with exactly the same conditions before reoxidation. This shows that metallic sites are responsible for the catalytic activity, in agreement with recent results on Pd/Al_2O_3 [21]. Note that bismuth was reduced slowly but not completely after the temperature was increased to 60 °C (8), affording a higher catalytic activity.

Despite the changes in operation conditions and catalytic activity (online FTIR) and the variation in the oxidation state of bismuth, EXAFS spectra at the Pd K-edge corresponding to points (3), (5), and (7) of Fig. 8, combined with the k^3-weighted Fourier-transformed data, demonstrate that the state of the Pd component remained largely insensitive to reoxidation (Fig. 9). Thus, Bi seems to protect palladium from oxidation, as has been observed in the oxidation of glucose [49] and 1-phenylethanol [23]. The reducing power of benzyl alcohol is superior to that of 1-phenylethanol, and thus it keeps Pd (and partially Bi) constantly in the reduced state.

4. Discussion

The aerobic oxidation of benzyl alcohol proceeds on reduced Pd sites according to a two-step dehydrogenation mechanism [1,2]: adsorption of the alkoxide, followed by β-H elimination to afford the aldehyde product. The major role of adsorbed oxygen is to oxidize the co-product hydrogen, thus shifting the equilibrium toward the carbonyl compound. The reaction mechanism is a network of side reactions whose occurrence strongly depends on the experimental conditions. Recent ATR-IR studies on Pd/Al_2O_3 during alcohol oxidation have uncovered different surface species [27], including adsorbed and dissolved benzaldehyde (dehydrogenation of benzyl alcohol), CO (decarbonylation of benzaldehyde), and benzoate (benzaldehyde oxidation and disproportionation). Toluene can be found by GC analysis during dehydrogenation due to the reactive adsorbed hydrogen present on the noble metal surface [27]. The disappearance of adsorbed CO with admission of oxygen [29,50] to the flowing solution and the formation of surface water obviously suggest oxidation of CO and adsorbed hydrogen (from dehydrogenation reactions). Water accumulation on the

catalyst surface theoretically formed in equimolar amount to the carbonyl compound is responsible for accelerating the hydration of the aldehyde carbonyl group to the acid. Therefore, this provides indirect evidence for the increasing catalyst potential decreasing the dehydrogenation rate.

The present study shows that Bi has a strong effect on both the structure and the surface species, accompanied by improvements in both selectivity and activity. The combination of ATR-IR with XAS spectroscopy and online monitoring of the catalytic activity was crucial to obtain complementary information on the particles and the surface, thus providing structure–activity relationships. This allows for the simultaneous correlation among the evolution of the surface species, the oxidation state of the metal(s), and the catalytic activity. It should be noted, however, that the strict comparison of ATR-IR and XAS data is meaningful to only a certain extent because of the different designs of the two spectroscopic cells, which likely affect the mass transport of reactants and products to and away from the catalyst. This is best observed in the deactivation that can be followed in the ATR-IR spectra (Fig. 7), but must be induced in the XAS experiments (Fig. 8).

CO adsorption from liquid-phase shows that Pd and Bi do not alloy, due to the very mild conditions under which Bi deposition and more importantly, Bi reduction are performed. Thus, both techniques suggest that the origin of the promotion effect is primarily geometric (site blocking). The fraction of Pd exposed to the liquid environment is diminished compared with the original Pd/Al_2O_3. This is demonstrated by the lower availability of adsorption sites on $Pd–Bi/Al_2O_3$ for multibonded CO compared with the almost unperturbed CO_L species. The fact that Bi deposits preferentially on Pd is in agreement with the preferential and irreversible adsorption of Bi on Pt(111) electrodes [51,52] and already indicates that large faces are likely favored over defect sites. It should be noted, however, that the behavior of Bi-promoted Pd/Al_2O_3 and Pt/Al_2O_3 toward oxidation of a specific alcohol also may be strikingly different [14].

The geometric blocking of Pd by Bi has an obvious influence on the catalytic activity of $Pd–Bi/Al_2O_3$. The ATR-IR data obtained during reaction indicate that the addition of Bi increases both activity and selectivity. The effect of the presence of Bi on selectivity is indicated mainly by the inhibition of side reactions like product decarbonylation and hydration. Thus the reduced amount of available Pd owing to Bi-blocking is balanced, resulting nevertheless in an equal product yield. Thus, Bi improves selectivity under anaerobic conditions. Inhibition of the hydration reaction, especially under oxidative conditions, intrinsically implies that Bi also better regulates the transfer of oxygen from the liquid phase to the active metal sites, as proposed previously [23,49]. It should be noted that an oxygen mass transfer limitation is required in alcohol oxidation [16,53]. An excessive amount of oxygen must not reach the Pd surface, but oxygen is required for the dehydrogenation step to clean the Pd surface of, for example, adsorbed hydrogen and CO. In accordance with this, the XAS experiment shown in Fig. 8 demonstrates that metallic Pd is required for higher catalytic activity, as postulated in the dehydrogenation mechanism. Activity is inferior after partial reoxidation of Bi and likely of surface Pd by oxygen [21]. The amount of oxygen on the catalyst surface can be maintained longer at its optimum on $Pd–Bi/Al_2O_3$ than on Pd/Al_2O_3. This is demonstrated by the ATR-IR data shown in Fig. 7, by the online FTIR measurements displaying a broader activity window for $Pd–Bi/Al_2O_3$, but especially by the XAS experiments in which Bi deposited on the Pd particles selectively reoxidized before the noble metal (Fig. 8) similar to the case of 1-phenylethanol [23]. Because XAS is surface-sensitive only with respect to Bi [23], it remains possible that surface Pd is oxidized but is not detected.

The fate of Bi in the oxidation of benzyl alcohol also appears to be affected by the alcohol. The high reduction potential of benzyl alcohol compared to 1-phenylethanol favors the metallic state of Pd. Both ATR-IR [29] and XAS [23] experiments on the selective oxidation of 1-phenylethanol provided evidence that the activity of reduced Pd is inferior compared with benzyl alcohol.

The aforementioned observations suggest that Bi controls oxygen supply to the active sites avoiding rapid reoxidation of Pd and strongly influences the product distribution. An earlier ATR-IR investigation of the Pd/Al_2O_3 catalyst also revealed that different Pd sites can be responsible for a specific reaction pathway [28]. Benzyl alcohol dehydrogenation is rather structure-insensitive, that is, it occurs evenly on the different sites of a Pd particle. On the other hand, it was shown that product decarbonylation seems to be favored on extended Pd domains, such as (111) surfaces. Evidence for this was the formation of CO_{B3} species (as in Fig. 6) during reaction and the dehydrogenation proceeding only when the CO_{B2} sites [predominantly edges and (100) faces] become free. Interestingly, the ATR-IR spectra displayed in Fig. 6 show negligible formation of CO during the dehydrogenation of benzyl alcohol on $Pd–Bi/Al_2O_3$. In agreement with the principle that Bi is located preferentially on the Pd particles, the absence of CO during dehydrogenation can be related to the preferential blocking of large Pd faces by Bi, resulting in the suppression of product decarbonylation and, consequently, greater selectivity. This behavior makes Pd–Bi-type materials attractive catalysts for industrial applications.

5. Conclusion

Insight into structure–performance relationships of Bi-promoted Pd/Al_2O_3 has been gained using a combination of ATR-IR and XAS spectroscopy and online monitoring of products in the liquid phase. This approach allows simultaneous monitoring of the surface species evolved during reaction and of the structure (oxidation state) of the catalyst under working conditions. Although a complete understanding of the promoter effect frequently observed in aerobic oxidation of alcohols has to account for a number of phenomena, the combined spectroscopic approach applied revealed new facets of Bi promotion in the aerobic oxidation of benzyl alcohol.

The effect of Bi promotion on the evolution of surface species on a Pd/Al_2O_3 catalyst prepared by selective deposition of Bi appears to be a geometric effect with two major consequences on the selective aerobic oxidation of benzyl alcohol.

Under dehydrogenation conditions, Bi inhibits side reactions and increases selectivity but likely does not affect the rate of dehydrogenation. Under oxidative conditions, Bi acts on the supply of oxygen to the catalyst surface, regulating it in such a way that the promoter oxidizes before the metal. From a chemical standpoint, this implies that side reactions are inhibited (e.g., product oxidation) with a consequent increase in selectivity and a prolonged catalytic activity.

Although promotion is exerted already under anaerobic conditions, selective aerobic oxidation of benzyl alcohol can be interpreted with a model of the promoter effect similar to that observed for oxidation of cinnamyl alcohol on Bi-promoted Pt/Al_2O_3 [14]; that is, Bi promotion is related predominately to the presence of oxygen.

This study, along with a previous study on the determination of active metal sites [28], provides input for rational catalyst design not only for the specific reaction selected here and should initiate interest for the *in situ* spectroscopic investigation of other catalytic systems combining XAS and infrared spectroscopy under working conditions.

Acknowledgments

Financial support for this work was provided by the Foundation Claude and Giuliana. The authors thanks ANKA (Karlsruhe, Germany) and HASYLAB at DESY (Hamburg, Germany) for the beam time for the *in situ* XAS investigations, Electron Microscopy ETH Zurich (EMEZ) for the TEM measuring time, M. Hermann and Dr. A. Webb (HASYLAB) for help and support during the beam time, Dr. M. Caravati for support during the measurements, and P. Haider for the catalytic testing. C.M. received a scholarship from the University of Milan. The work at the synchrotron radiation sources was supported by the European Community—Research Infrastructure Action under the FP6 program, "Structuring the European Research Area" (through the Integrated Infrastructure Initiative "Integrating Activity on Synchrotron and Free Electron Laser Science," contract RII3-CT-2004-506008).

References

[1] M. Besson, P. Gallezot, Catal. Today 57 (2000) 127.
[2] T. Mallat, A. Baiker, Chem. Rev. 104 (2004) 3037.
[3] T. Mallat, Z. Bodnar, A. Baiker, Stud. Surf. Sci. Catal. 70 (1993) 337.
[4] F. Alardin, B. Delmon, P. Ruiz, M. Devillers, Catal. Today 61 (2000) 255.
[5] G. Li, D.I. Enache, J. Edwards, A.F. Carley, D.W. Knight, G.J. Hutchings, Catal. Lett. 110 (2006) 7.
[6] D.I. Enache, J.K. Edwards, P. Landon, B. Solsona-Espriu, A.F. Carley, A.A. Herzing, M. Watanabe, C.J. Kiely, D.W. Knight, G.J. Hutchings, Science 311 (2006) 632.
[7] N. Dimitratos, J.A. Lopez-Sanchez, D. Lennon, F. Porta, L. Prati, A. Villa, Catal. Lett. 108 (2006) 147.
[8] N. Dimitratos, A. Villa, D. Wang, F. Porta, D. Su, L. Prati, J. Catal. 244 (2006) 113.
[9] L. Prati, A. Villa, C. Campione, P. Spontoni, Top. Catal. 44 (2007) 319.
[10] T. Mallat, A. Baiker, Catal. Today 19 (1994) 247.
[11] P.C.C. Smits, B.F.M. Kuster, K. van der Wiele, H.S. van der Baan, Carbohydr. Res. 153 (1986) 227.
[12] M. Akada, S. Nakano, T. Sugiyama, K. Ichitoh, H. Nakao, M. Akita, Y. Moro-oka, Bull. Chem. Soc. Jpn. 66 (1993) 1511.
[13] H.H.C.M. Pinxt, B.F.M. Kuster, G.B. Marin, Appl. Catal. A 191 (2000) 45.
[14] C. Keresszegi, T. Mallat, J.D. Grunwaldt, A. Baiker, J. Catal. 225 (2004) 138.
[15] K. Heyns, H. Paulsen, Adv. Carbohydr. Chem. 17 (1962) 169.
[16] R. DiCosimo, G.M. Whitesides, J. Phys. Chem. 93 (1989) 768.
[17] T. Mallat, Z. Bodnar, P. Hug, A. Baiker, J. Catal. 153 (1995) 131.
[18] R.M. Souto, J.L. Rodriguez, E. Pastor, Langmuir 16 (2000) 8456.
[19] A.P. Markusse, B.F.M. Kuster, J.C. Schouten, Catal. Today 66 (2001) 191.
[20] V.R. Gangwal, B.G.M. vanWachem, B.F.M. Kuster, J.C. Schouten, Chem. Eng. Sci. 57 (2002) 5051.
[21] J.D. Grunwaldt, M. Caravati, A. Baiker, J. Phys. Chem. B 110 (2006) 25586.
[22] C. Keresszegi, J.D. Grunwaldt, T. Mallat, A. Baiker, Chem. Commun. (2003) 2304.
[23] C. Keresszegi, J.-D. Grunwaldt, T. Mallat, A. Baiker, J. Catal. 222 (2004) 268.
[24] N.J. Harrick, Internal Reflection Spectroscopy, Interscience, New York, 1967.
[25] T. Bürgi, A. Baiker, Adv. Catal. 50 (2006) 227.
[26] T. Bürgi, M. Bieri, J. Phys. Chem. B 108 (2004) 13364.
[27] C. Keresszegi, D. Ferri, T. Mallat, A. Baiker, J. Phys. Chem. B 109 (2005) 958.
[28] D. Ferri, C. Mondelli, F. Krumeich, A. Baiker, J. Phys. Chem. B 110 (2006) 22982.
[29] C. Keresszegi, D. Ferri, T. Mallat, A. Baiker, J. Catal. 234 (2005) 64.
[30] T. Bürgi, R. Wirz, A. Baiker, J. Phys. Chem. B 107 (2003) 6774.
[31] A. Gisler, T. Buergi, A. Baiker, Phys. Chem. Chem. Phys. 5 (2003) 3539.
[32] D. Baurecht, G. Reiter, N. Hassler, M. Schwarzott, U.P. Fringeli, Chimia 59 (2005) 226.
[33] J.-D. Grunwaldt, C. Keresszegi, T. Mallat, A. Baiker, J. Catal. 213 (2003) 291.
[34] T. Ressler, J. Synch. Rad. 5 (1998) 118.
[35] S.I. Zabinsky, J.J. Rehr, A. Ankudinov, R.C. Albers, M.J. Eller, Phys. Rev. B 52 (1995) 2995.
[36] P. Haider, A. Baiker, J. Catal. 248 (2007) 175.
[37] T. Mallat, Z. Bodnar, A. Baiker, O. Greis, H. Struebig, A. Reller, J. Catal. 142 (1993) 237.
[38] S. Karski, I. Witonska, J. Mol. Catal. A 191 (2003) 87.
[39] J. Goetz, M.A. Volpe, A.M. Sica, C.E. Gigola, R. Touroude, J. Catal. 167 (1997) 314.
[40] M. Wenkin, P. Ruiz, B. Delmon, M. Devillers, Stud. Surf. Sci. Catal. 108 (1997) 391.
[41] S. Karski, J. Mol. Catal. A 253 (2006) 147.
[42] T. Miyake, A. Hattori, M. Hanaya, S. Tokumaru, H. Hamaji, T. Okada, Top. Catal. 13 (2000) 243.
[43] T. Lear, R. Marshall, J.A. Lopez-Sanchez, S.D. Jackson, T.M. Klapoetke, M. Baeumer, G. Rupprechter, H.-J. Freund, D. Lennon, J. Chem. Phys. 123 (2005) 174706.
[44] E. Groppo, S. Bertarione, F. Rotunno, G. Agostini, D. Scarano, R. Pellegrini, G. Leofanti, A. Zecchina, C. Lamberti, J. Phys. Chem. C 111 (2007) 7021.
[45] M. Bäumer, H.J. Freund, Prog. Surf. Sci. 61 (1999) 127.
[46] A. Palazov, C.C. Chang, R.J. Kokes, J. Catal. 36 (1975) 338.
[47] H.E. van Dam, A.P.G. Kieboom, H. van Bekkum, Appl. Catal. 33 (1987) 361.
[48] P.J.M. Dijkgraaf, M.J.M. Rijk, J. Meuldijk, K. van der Wiele, J. Catal. 112 (1988) 329.
[49] M. Besson, F. Lahmer, P. Gallezot, P. Fuertes, G. Flèche, J. Catal. 152 (1995) 116.
[50] C. Keresszegi, T. Bürgi, T. Mallat, A. Baiker, J. Catal. 211 (2002) 244.
[51] M. Ball, C.A. Lucas, N.M. Markovic, B.M. Murphy, P. Steadman, T.J. Schmidt, V. Stamenkovic, P.N. Ross, Langmuir 17 (2001) 5943.
[52] P. Rodriguez, J. Solla-Gullon, F.J. Vidal-Iglesias, E. Herrero, A. Aldaz, J.M. Feliu, Anal. Chem. 77 (2005) 5317.
[53] J.H.J. Kluytmans, A.P. Markusse, B.F.M. Kuster, G.B. Marin, J.C. Schouten, Catal. Today 57 (2000) 143.